



Smouldering in fixed beds of oil shale grains. A three-dimensional microscale numerical model

G. Debenest , V. Mourzenko & J. Thovert

To cite this article: G. Debenest , V. Mourzenko & J. Thovert (2005) Smouldering in fixed beds of oil shale grains. A three-dimensional microscale numerical model, Combustion Theory and Modelling, 9:1, 113-135, DOI: [10.1080/13647830500052123](https://doi.org/10.1080/13647830500052123)

To link to this article: <http://dx.doi.org/10.1080/13647830500052123>



Published online: 08 Nov 2010.



Submit your article to this journal [↗](#)



Article views: 86



View related articles [↗](#)



Citing articles: 15 View citing articles [↗](#)

Smouldering in fixed beds of oil shale grains. A three-dimensional microscale numerical model

G. DEBENEST, V. V. MOURZENKO, and J.-F. THOVERT*

Laboratoire de Combustion et de Détonique, ENSMA, 1 Avenue Clément Ader, B. P. 40109,
Futuroscope Chasseneuil du Poitou, Cedex 86961, France

(Received 15 June 2004; accepted 28 October 2004)

A three-dimensional, microscale numerical model for the simulation of smouldering in fixed beds of solid fuels is presented. It solves the local governing equations, and therefore explicitly accounts for the coupling of the transport and reaction mechanisms on the microscopic scale. This article describes the conceptual and numerical apparatus and provides illustrative examples of calculations. Extensive applications will be presented in two companion papers.

1. Introduction

Smouldering in porous media occurs in a variety of situations, such as waste incineration, fire hazards, or the burning of solid fuels for industrial purposes. From a practical point of view, different aspects can be regarded as desirable or as an inconvenience in each of these situations. However, in all these problems, the processes take place in a domain with a very complex geometry; they involve many transport mechanisms which are coupled on the microscale with various chemical reactions.

Since a detailed description is very difficult, a macroscopic point of view is adopted in many studies, whereby the medium is regarded as a continuum. The equations then involve various effective parameters and they relate macroscopic fields that represent averages of local quantities over a volume significantly larger than the characteristic length scale of the microstructure (e.g. a typical grain size). However, the validity of such an upscaled description is an open question in many cases; in addition, the determination of the effective coefficients, when applicable, is by no means trivial.

These questions can only be answered by examining the details of the processes on the microscale, as is the rule for any homogenized model. This was one of our motivations for the development of a numerical simulation tool based on a microscopic description, where the local equations are solved in a detailed discretized image of the microstructure. Another reason is the intrinsic interest of such a model for the investigation of situations that we know beforehand cannot be properly described by macroscopic models (e.g. near singularities like walls, obstacles, heterogeneities, or in an entry region), or for parametric studies that may be easier to carry out numerically than experimentally. Finally, a microscopic approach gives

*Corresponding author. E-mail: thovert@lcd.ensma.fr

access to local information which can be highly interesting. For instance, the chemical processes are controlled by local thermochemical conditions, which are only coarsely described by volume averaged quantities.

Hence, we address in this series of articles the simulation of smouldering in porous solid fuels, by use of a fairly general 3D numerical simulation tool, operating on the microscopic scale and accounting as much as possible for the interactions between local transport and reaction mechanisms. This is of course a formidable task. Given the geometrical complexity of the microstructure and the contrast between the microscale and the minimum size of the overall simulation domain to consider, many simplifications had to be made. However, care was taken to preserve the main feature that we want to investigate, that is the coupling on the microscale of the transport and reaction processes, which determines the whole behaviour of the system.

The present paper is devoted to the description of the numerical model, and to the presentation of a few illustrative applications. A wide range of situations is investigated in a second article (Debenest *et al.* [1]) which provides an insight into the variety of the possible behaviours. Two-dimensional situations will be preferred then, because they allow for faster computations and thereby for an easier sweep of the parameters, but most importantly because of the easier graphical display of the results. A third paper will address the full 3D simulation of a reference situation, with a narrower range of parameters, but with a greater emphasis put on realism.

This paper is organized as follows. In the next section, the problem is stated in more detail, with reference to a situation which corresponds to an actual experimental set-up, and a literature survey is conducted. The local mechanisms and the associated microscopic formulation of the problem are discussed in section 3. All the simplifications and approximations which are used in the model are thoroughly listed and commented. At this point, we end up with the simplified physico-chemical model which is addressed numerically in the rest of this work. Its numerical implementation is described in section 4. We try to survey all aspects of the simulation tool, which is a rather large and complex piece of software, but for the sake of concision, we skip most of the technical details and validation tests, which are given in full by Debenest [2]. Finally, illustrative examples of results are given in section 5, and desirable extensions to the model are discussed.

2. General

2.1 *General description of the problem*

As already stated, smouldering occurs in a variety of situations and materials. While a macroscopic description raises similar conceptual and theoretical questions in all cases, the details of the mechanisms vary and we need to be more specific in order to devise a numerical simulation tool. We consider here smouldering in fixed beds of ground oil shale grains. As a rule, the general setting, the materials and the operating parameters of a lab-scale experiment (Ahd *et al.* [3]) are used as a reference situation, which ensures that our calculations are conducted in a realistic situation.

Oil shales, among other solid fuels, correspond to an intermediate level of difficulty. From the chemical point of view they are more complex than coal, for instance, since they contain a variety of organic compounds. On the other hand, an important fraction of nearly inert inorganic matrix induces the simplifying feature that the geometry of the packed bed is modified very little by the smouldering process, unlike for most other fuels which leave a small amount of unburned solid residue.

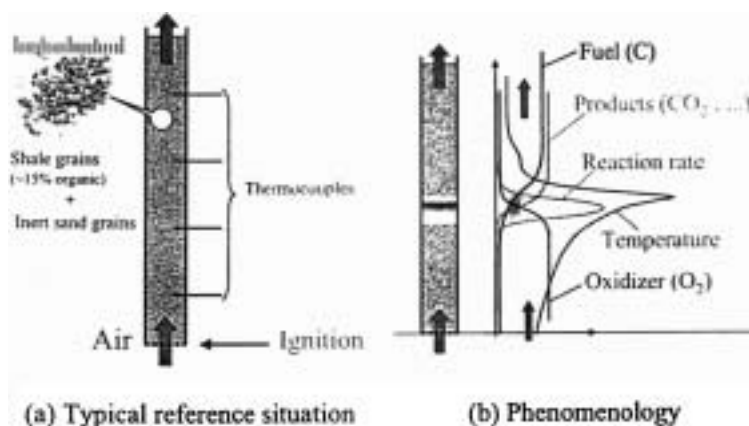


Figure 1. Sketch of the experimental set-up.

The experimental set-up is sketched in figure 1. Ground Moroccan oil shale is packed in a vertical cylindrical column. The grains have irregular shapes but moderate aspect ratios, and a typical diameter $\Phi \approx 600 \mu\text{m}$; they may be mixed with inert sand grains, with similar geometrical characteristics. The column inner diameter is 28.3 mm. It is equipped with a series of thermocouples, so that temperature at serial positions can be recorded as a function of time. Air is blown from the bottom, where ignition is performed. The flow rate can be varied, but the Reynolds number Re never exceeds a few units. Most of the material physical properties are known, at least approximately; however, the amount of kerogen in the shale and its composition are not well quantified. Note that there are only two operating parameters, namely the gas flow rate and the volume fraction of inert sand in the packed bed.

Let us add a few phenomenological observations (see figure 1(b)). During an experiment, a reaction front propagates upwards. It can be followed visually, with a glowing layer about 3Φ thick. The temperature measured in this zone may rise up to $700\text{--}900^\circ\text{C}$ above room temperature. However, what this temperature represents is not clear. The thermocouples sit in the gas, and they are about 2Φ in diameter, which means that their signals are probably a complex mixture of spatial and temporal integrations. This is one of the points that our simulations could help elucidate.

Pyrolytic reactions take place downstream of the front. There, the kerogen decomposes into various gaseous compounds, which are taken away by the flow, and a solid carbon char, that later reacts with the oxygen. Since the fraction of kerogen in the shale is moderate, the geometry of the bed is almost unchanged during the process; the subsidence does not exceed a few percent of the overall bed height.

2.2 Literature survey

The literature on the modelling of smouldering processes based on a microscopic description is rather scarce, and we are not aware of any prior attempt at the level of detail that is aimed at here. In a founding paper, Ohlemiller [4] gave a thorough review of the coupled chemical and physical processes involved in smouldering, and proposed a general mathematical model for a packed-bed reactor, which meticulously accounted for all the transport mechanisms on the pore and grain scale, and for complex chemical processes. The authors themselves judged the model intractable, which was certainly true by then. Moallemi *et al.* [5] still professed the same opinion nearly a decade later, and indeed this approach has lain dormant until very recently.

Lu and Yortsos [6] present numerical simulations, where the porous medium is represented by a simple dual capillary network. The gas flows through the pore network, heat is conducted by the solid network, reaction takes place in the sites of the pore network, the concentrations and the temperature are uniform in the network sites, and all the transfers and couplings are modelled by effective coefficients. Hence, this cannot be regarded as a truly microscopic approach. Redl [7] comes closer to this objective. His flow simulations, based on a lattice-Boltzmann method, really operate in the 3D pore space, and the energy transport equation is solved both in the gas and solid domains on the microscopic scale. However, the solid oxidation reaction is modelled by a homogeneous reaction in the bulk of the gas phase, which cancels most of the local coupling of the transport and reaction processes. We have to also mention here the work of Hackert *et al.* [8], in the different but related context of filtration combustion in porous burners, which presents truly microscopic simulations, with a full description of the local transport and reaction coupling, although in simple 2D configurations.

Owing to this difficulty, most of the numerical or analytical literature about smouldering is based on a macroscopic approach, by use of an homogenized description. Two fundamental papers are of great importance for understanding the underlying assumptions and approximations in this framework, and of their limitations, namely the aforementioned review article by Ohlemiller [4], and that by Oliveira and Kaviani [9]. The latter makes an inventory of the various mechanisms that may lead to local thermal or chemical disequilibrium, of their impact on the combustion process and of their modelling in upscaled descriptions. They also examine under which conditions a homogenized description is possible. Both of them clearly expose the shortcomings of the macroscopic description and insist on the need for detailed local investigations in many situations.

The classical macroscopic approach is perfectly illustrated by a series of enlightening articles by a group very active in this field (Schult *et al.* [10, 11]; Shkadinsky *et al.* [12]; Aldushin and Matkowsky [13]; Aldushin *et al.* [14]; Aldushin and Matkowsky [15]; Whale and Matkowsky [16]). Most papers make use of a quite typical set of simplifying assumptions (quoted from Schult *et al.* [10]):

To simplify the analysis, we assume that (1) the gas and solid phases are in local thermodynamic equilibrium so that a single temperature model is possible, (2) radiation heat transfer is modeled by a diffusion approximation, (3) the solid phase is stationary and non deforming, (4) Fick's law describes the diffusion of oxidizer through the gas with the quantity $D\rho_g$ constant, (5) the flow resistance through the porous sample is small enough that pressure is essentially constant, (6) the sample is sufficiently long that end effects are negligible and do not influence the transport of heat or oxidizer, (7) the activation energy of the reaction is large.

We should also mention that their chemical model involves a single one-step heterogeneous oxidative reaction, and that the analytical treatment is conducted in the limit of a very narrow reaction zone.

It should be noted that two important simplifications are made here, relative to behaviours which result from the complex coupling of local mechanisms. The first one is (1), whereby the solid/gas heat exchanges are regarded as very fast. The second one is a similar assumption (which does not appear in the previous list) that diffusive transfer of the oxidizer from the bulk of the gas phase to the solid surface is also very fast, so that its concentration is locally uniform across the pore space and its transverse variations do not have to be accounted for in the reaction kinetics.

These assumptions were partly lifted in some papers. In particular, Whale and Matkowsky [16] present one of the most complete models; it is one of the very few in the literature where local thermal equilibrium is not assumed from the start. Instead, the solid matrix and the gas are treated as two intermixed continua in a two-temperature model. In addition, the oxidizer is not supposed to redistribute instantaneously across the pores. The effects of these finite rates of the transfers between the phases are embodied in two effective heat and mass transfer

coefficients, α and β , which play a direct and important role in the model for the reaction kinetics. However, there is no way to guess the proper setting of these coefficients, and the authors eventually treat only limiting cases where either α or β is very large (i.e. when the system is in local thermal equilibrium, or the oxidizer diffusion is instantaneous).

Of course, many other effective transport coefficients are involved in the governing equations, such as the macroscopic conductivity for the solid or the apparent diffusion coefficient of the oxidizer in the gas. These may also cause some trouble. For instance, Aldushin and Matkowsky [13] use the argument that the Péclet number is large so that the diffusive terms for the heat and oxidizer transports in the gas can be neglected compared to the convective ones. This overlooks the influence of hydrodynamic dispersion, which is then much larger than diffusion.

All the analytical or numerical studies of smouldering from a macroscopic point of view in the literature are based on sets of assumptions which are more or less equivalent to the previous ones. For instance, Moallemi *et al.* [5], who address two-dimensional smouldering processes, and Akkutlu and Yortsos [17], who take transverse heat losses into account, use a set of approximations which is essentially that of Schult *et al.* [10]. Note that similar approaches with the same shortcomings are used for the model of filtration combustion of premixed gaseous mixtures in porous burners (see Deshaies and Joulin [18]; Zhdanok *et al.* [19]; Henneke and Ellzey [20]).

In summary, the macroscopic approach suffers from two drawbacks. There are situations where its upscaled formulation is not appropriate, and they are difficult to discriminate from within. Then, the values of the effective coefficients which are required for its implementation are difficult to figure out. Both problems can be solved only by investigating the detailed mechanisms and their coupling on the microscopic scale.

2.3 Objectives

Given this, our primary objective was to devise a numerical simulation tool which meets the following specifications. It should operate on the microscopic scale, in a realistic 3D digital image of the porous medium microstructure, and solve the local governing equations. Simplifications are unavoidable in view of the complexity of the problem, but we restrain as much as possible from introducing in the formulation any effective behaviour or coefficient, if they do not result from a careful preliminary analysis which generally involves an upscaling based on the resolution of a local problem. The guiding idea is to preserve the coupling of the various mechanisms on the microscopic scale (transports and reactions), and to account for the competitions of the numerous time scales which govern them.

In practice, the model should incorporate a detailed description of the following processes: the fluid flow (oxidizing gas and reaction products); the convective/diffusive transport of chemical species to and from the reaction sites; the heat production and transport, by conduction/convection and possibly radiation; the chemical reactions; the evolution of the material and of its properties.

As a direct simulation tool, this apparatus would allow us to quantify the influence of operating parameters, such as the flow regime, the fraction of inert, and more generally to conduct parametric studies for the optimization of the process, sometimes in an easier and more versatile way than by physical experimentation. Because of its microscopic and three-dimensional character, it would also allow us to address tasks which cannot be performed by using a macroscale model. This includes providing elements for the assessment of macroscopic formulations and estimating the effective coefficients involved in these formulations, investigating the influence of singularities (obstacles, walls, etc.) or more generally of microscale

heterogeneity, and possible instabilities of the reaction front, in some regimes. Finally, one might take advantage of the local knowledge of the thermochemical conditions at the reaction sites to investigate problems such as the emission of noxious species.

The numerical model described in this paper meets the specifications enunciated above, with a single exception regarding the chemical model. It is not complete yet, since it only implements the physico-chemical model described in section 3.5, which makes use of many simplifications, but its design is flexible enough to allow for many desirable extensions, especially on the chemical side. Some of them are currently being implemented, others are planned for the near future. Still, the model as it stands is sufficiently rich to provide interesting and new results. A few illustrative cases are presented in section 5, and extensive applications will be presented by Debenest *et al.* [1] and in forthcoming papers.

3. Survey of the local mechanisms and microscopic formulation

In this section, we examine in detail the numerous mechanisms that play a role on the microscopic scale, introduce various approximations and simplifying assumptions, and finally provide a set of governing equations, which summarizes the problem to be solved in the numerical simulations.

3.1 Survey of the mechanisms

Four main zones can be found in the bed, which move downstream as the process progresses. These are: an entry region, where the fuel is nearly exhausted or the temperature is too low to sustain any chemical reaction, and where the air is preheated; a hot reaction zone, where the oxidizer meets and reacts with the carbon char left in the shale by the pyrolysis; a pyrolysis region (which may overlap with the former), where thermal cracking of the organic matter in the shale yields gaseous species that are carried away by the flow, and a carbon char, that stays in the shale grains; a final downstream region, too cold to induce any chemical process, which the flow simply traverses, conveying heat and reaction products away from the system.

In most of this work, attention is focused on the reaction zone, where the couplings between transport and reaction mechanisms have the most critical influence. Less attention is paid to the first, third and fourth region, although they cannot be totally disregarded, because they provide the boundary conditions for the area of interest. In the current version of the model, it is assumed that the combustion and pyrolysis zones do not overlap. Hence, the gaseous pyrolytic products are washed away by the flow before they have the opportunity to react with the oxygen, and therefore, we do not need to keep track of them in the calculations. Note that this assumption is subject to *a posteriori* verification, and it is indeed supported in most cases by the results of our simulations, since the oxygen concentration profile in the reaction zone decays much faster than the temperature profile. The introduction of an explicit account of pyrolysis is planned for the near future.

The rest of this section is devoted to the description of the minimal set of physico-chemical processes necessary for non-trivial microscopic simulations of smouldering. The sketch in figure 2 is a close-up of the microstructure that summarizes the various mechanisms which are considered in the model and detailed in the following subsections. The gas flows between the grains of the bed, and conveys heat and several chemical species (oxygen and various reaction products). Heat is also conducted by the solid phase. Combustion is regarded as a heterogeneous reaction on the surface of the shale grains, and pyrolysis is supposed to occur somewhat downstream of the combustion zone. The carbon content is nearly exhausted on the upstream side, as well as the oxygen concentration in the gas on the downstream side. This pattern progressively shifts in the downstream direction as the process continues.

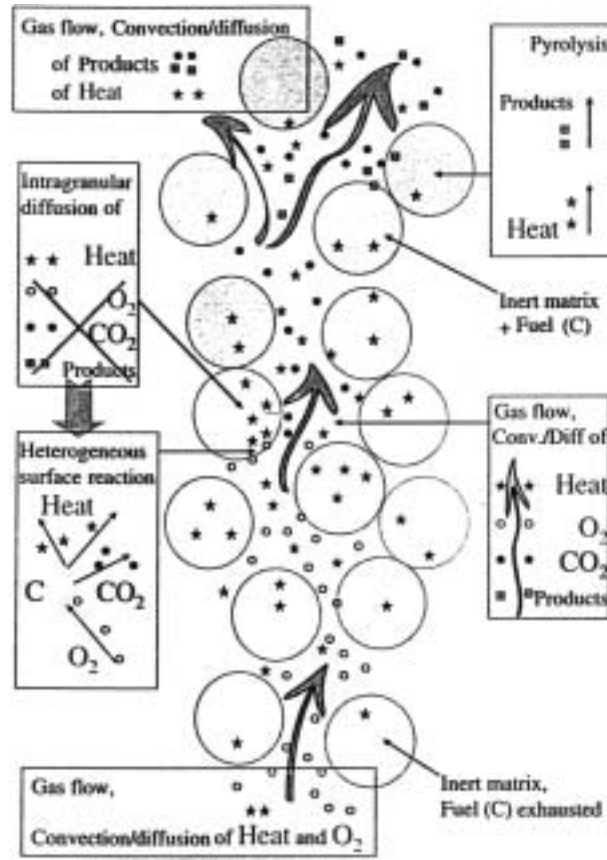


Figure 2. Close-up of the bed microstructure, and illustration of the mechanisms included in the microscopic formulation of the problem. The symbols refer to the transported quantities: heat (\star), oxygen (\circ), carbon dioxide (\bullet) and pyrolytic products (\blacksquare).

Let us introduce a few notations for later use. The domain \mathcal{V} decomposes into pore and solid spaces, denoted by \mathcal{P} and \mathcal{S} , respectively, with $\mathcal{V} = \mathcal{P} \cup \mathcal{S}$, and the pore and solid spaces are denoted by \mathcal{P} and \mathcal{S} , respectively, with $\mathcal{V} = \mathcal{S} \cup \mathcal{P}$, and the pore volume fraction (i.e. the porosity) is denoted by $\epsilon = \mathcal{P}/\mathcal{V}$. The pore/solid interface is denoted by \mathcal{I} with normal vector (into the pores) $\mathbf{n}_{\mathcal{I}}$. When necessary, we may distinguish the oil shale and the inert solid by indices s and i , respectively, with $\mathcal{S}_s \cup \mathcal{S}_i = \mathcal{S}$ and $\mathcal{I}_s \cup \mathcal{I}_i = \mathcal{I}$.

3.2 Gas flow

The solid phase is regarded as impermeable with respect to the gas flow. Thus, the flow in the intergranular pore space \mathcal{P} is governed by the Navier-Stokes equations, supplemented with a no-slip condition on the solid surface \mathcal{I} , which actually reduces to a zero-velocity condition since \mathcal{I} is regarded as immobile. Indeed, the inert mineral matrix of the oil shale amounts to 80–90% of its volume, and the disappearance of the organic matter does not significantly alter the shape and size of the grains. Grain rearrangements, inducing geometry changes on a more global scale, are also ignored based on experimental observation.

In the reference experimental setup, the gas velocity and the associated pressure variations are small, and the gas can be regarded as an incompressible fluid. The Reynolds number Re (based on the typical grain size) is at most equal to a few units, and we may safely

assume that the flow remains laminar. In addition, we assume that inertia has little influence on the flow field structure, with the consequence that the quadratic term in the Navier-Stokes momentum equation can be neglected. This was checked by comparing the flow fields obtained by solving the Navier-Stokes equations with Re up to ten, which highly exceeds the range in the experiment [2].

Finally, the strongest approximation is to ignore the dependence of the gas density and viscosity on its temperature and on its composition. This greatly simplifies the simulations since it actually decouples the flow problem from the reaction processes. In the present case, with a constant imposed global flow rate, it even means that the flow field is stationary. Hence, the gas velocity field can be determined prior to any other calculations, and used throughout the simulations. The gas flow is eventually governed by the Stokes equations,

$$\nabla p = \mu \nabla^2 \mathbf{v}, \quad \nabla \cdot \mathbf{v} = 0, \quad \text{in } \mathcal{P} \quad (1a)$$

$$\mathbf{v} = 0, \quad \text{on } \mathcal{I} \quad (1b)$$

where \mathbf{v} is the local velocity, μ is the dynamic viscosity and p is the pressure. Since we are mostly interested in a precise description of the reaction zone, we use the values of the gas physical constants that prevail in this area, i.e. their values for the typical temperature observed near the reaction front. The flow equations are complemented by the prescription of the global mass flow rate,

$$\rho \bar{\mathbf{v}} = \frac{\rho}{V} \int_{\mathcal{P}} \mathbf{v} d^3 \mathbf{r}, \quad (2)$$

where ρ is the gas density, $\bar{\mathbf{v}}$ is its seepage velocity, and \mathbf{r} is the position vector.

3.3 Transport of the gaseous chemical species

Several gaseous species are conveyed by the flowing gas. A common approximation is used for the description of their transport, namely that they are all treated as dilute components, i.e. that their diffusive fluxes do not alter the local barycentric velocity \mathbf{v} of the conveying fluid, which is the solution of the problem (1, 2). The main consequence is that their transports are all described by similar and mutually independent convection–diffusion equations. For the oxygen flow \mathbf{J}_O (and by straightforward analogy for all other transported gaseous species, such as reaction products), this yields

$$\frac{\partial c_O}{\partial t} + \nabla \cdot \mathbf{J}_O = 0, \quad \text{in } \mathcal{P} \quad (3a)$$

$$\mathbf{J}_O = \mathbf{v} c_O - D_O \nabla c_O, \quad \text{in } \mathcal{P} \quad (3b)$$

$$\mathbf{n}_{\mathcal{I}} \cdot \mathbf{J}_O = S_{O,\mathcal{I}}, \quad \text{on } \mathcal{I} \quad (3c)$$

where c_O is the concentration, D_O is the molecular diffusion coefficient, and $S_{O,\mathcal{I}}$ is a surface sink term, due to the chemical reaction on \mathcal{I}_s . D_O is taken constant in the simulations, just like the other gas physical parameters. The global boundary conditions are the concentration at the inlet and a sink condition located far enough from the reaction zone on the downstream side.

The dimensionless Péclet number, which compares the characteristic times for diffusion (Φ^2/D_O) and for convection (Φ^2/v^*), plays a central role in the convective–diffusive transport.

$$Pe_O = \frac{v^* \Phi}{D_O} \quad (4)$$

where v^* is the magnitude of the mean interstitial velocity v^* ,

$$v^* = \frac{1}{\mathcal{P}} \int_{\mathcal{P}} \mathbf{v} d^3\mathbf{r} = \frac{1}{\epsilon} \bar{\mathbf{v}}. \quad (5)$$

The Péclet number defined in equation (4) is relative to the oxygen, but similar numbers can be defined for all the transported species. However, they only differ by the molecular diffusion coefficient in the denominator, and thus they are all related to each other.

3.4 Heat transport

Unlike the gas and the various species that it conveys, heat can obviously enter and spread in the solid phase. Therefore, two equations have to be written, relative to convection–diffusion in the pore space and to conduction in the solid phase, which are coupled by temperature and flux continuity conditions at the interface \mathcal{I}

$$C_g \frac{\partial T_g}{\partial t} + \nabla \cdot \mathbf{J}_{T,g} = 0, \quad \mathbf{J}_{T,g} = C_g \mathbf{v} T_g - \lambda_g \nabla T_g \quad \text{in } \mathcal{P} \quad (6a)$$

$$C_s \frac{\partial T_s}{\partial t} + \nabla \cdot \mathbf{J}_{T,s} = 0, \quad \mathbf{J}_{T,s} = -\lambda_s \nabla T_s \quad \text{in } \mathcal{S} \quad (6b)$$

$$T_g = T_s, \quad \text{on } \mathcal{I} \quad (6c)$$

$$\mathbf{n}_{\mathcal{I}} \cdot (\mathbf{J}_{T,g} - \mathbf{J}_{T,s}) = S_{T,\mathcal{I}}, \quad \text{on } \mathcal{I} \quad (6d)$$

where t is the time, $S_{T,\mathcal{I}}$ is a source term on the interface, C_i is the volumetric heat capacity of phase i and λ_i its thermal conductivity, T_i is the temperature and $\mathbf{J}_{T,i}$ the heat flux. Let us also introduce for later use the thermal diffusion coefficients, $D_{T,i} = \lambda_i / C_i$. Again, the dependence of the physical parameters on the temperature and on the gas composition are ignored, and values corresponding to the typical temperature in the reaction zone are used in the simulations. By analogy with (4), a thermal Péclet number can be defined as

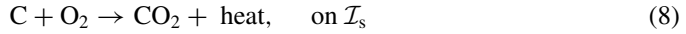
$$Pe_{T,g} = \frac{v^* \Phi}{D_{T,g}}. \quad (7)$$

The transport equations (6) are supplemented with initial and global boundary conditions. We generally start the simulations from an initial state where the solid is at room temperature. On the upstream boundary, an adiabatic condition is imposed on the solid; the injected air is at room temperature, but preheated air could be used just as easily. Transverse heat losses are not considered. Finally, the thermal boundary conditions on the downstream side are a sink at some distant location. Since this condition can have a significant influence in the reaction zone, an original technique was devised, which is described by Debenest *et al.* [1], whereby it can be shifted to a virtually infinite distance. The technique is based on the matching of the microscopic 3D model with a macroscale 1D equation in the far-field downstream region.

Note that equations (6) do not take radiative transfers into account, although they could be significant near the reaction zone. It is assumed that radiative exchanges between grains that face each other, which are generally in mechanical contact and therefore in conductive thermal contact, do not introduce a qualitative change in the heat transport process, as it would in a fluidized bed where conductive heat exchanges between the grains is impossible. Nevertheless, introduction of radiative transfers is one of the planned extensions of the numerical model.

3.5 Chemical model

A global ‘black-box’ approach is used to represent both the chemical reactions and the intra-granular transfers of the various species that are involved. In this model, which is basically a transposition of the ‘one-film model’ in chapter 10 of Turns [21], the whole reaction scheme is summarized by a global exothermal heterogeneous reaction that takes place on the surface \mathcal{I}_s of the shale grains,



There are two levels of simplification in this formulation. First, the carbon char is distributed in the volume of the grain. Thus, the oxygen has to diffuse through the intragranular microporosity in order to reach the reaction sites; conversely, the reaction products can only reach the intergranular domain by diffusing through the micropores. This introduces a delay between the instant when the oxygen reaches the grain surface and the instant when it reacts with carbon. We argue here that this time lag is short enough to be neglected without strongly affecting the global behaviour, as discussed in section 4.6.2. Hence, the intragranular transfers of the chemical species are not detailed. The other simplification is to reduce the reaction scheme to the single step reaction (8). It is likely that carbon monoxide is produced in a first step, on the char surface within the shale grains, which is later converted into carbon dioxide in the gas phase. However, since the second step is fast and probably takes place within the micropores in the grains, the chemical balance from the point of view of an observer out of the grain indeed reduces to (8).

The reaction kinetic of (8) is supposed to be of first order with respect to O_2 , with a rate coefficient given by Arrhenius law

$$r \propto H_C c_{\text{O}_2} e^{-E/RT}, \quad (9)$$

where H_C is a Heavyside step function accounting for the fuel exhaustion and R is the gas constant. Furthermore, the activation energy E is supposed to be large enough, so that a sharp transition exists between a low-temperature kinetically controlled regime, where the reaction rate is very small, and a high-temperature diffusionnally controlled regime. Thus, the kinetic law finally reduces to the following bimodal model,

$$\begin{cases} \text{negligible reaction} & \text{for } T < T_r \\ \text{diffusion limited reaction} & \text{for } T \geq T_r \end{cases} \quad (10)$$

where T_r is a threshold temperature.

The reaction induces the surface source and sink terms in equations (3c) and (6d). They are all proportional to the reaction rate r , with stoichiometric coefficients which are set according to (8). However, it is easier to rewrite them in the following way. Since the reaction is either negligible or diffusion-limited, we may replace the boundary condition for O_2 on \mathcal{I} in (3c) by

$$\begin{cases} \mathbf{n}_{\mathcal{I}} \cdot \mathbf{J}_{\text{O}} = 0 & \text{on } \mathcal{I}_i \\ \mathbf{n}_{\mathcal{I}} \cdot \mathbf{J}_{\text{O}} = 0 & \text{on } \mathcal{I}_s \text{ if } T < T_r \text{ or } H_C = 0 \\ c_{\text{O}} = 0 & \text{on } \mathcal{I}_s \text{ if } T \geq T_r \text{ and } H_C = 1. \end{cases} \quad (11a)$$

The source term in the counterpart of equations (3) for CO_2 is the opposite of the sink term for O_2 . The heat source $S_{T,\mathcal{I}}$ in (6d) is also proportional to the oxygen sink,

$$\mathbf{n}_{\mathcal{I}} \cdot (\mathbf{J}_{T_s} - \mathbf{J}_{T_s}) = \Delta h_c \mathbf{n}_{\mathcal{I}} \cdot \mathbf{J}_{\text{O}}, \quad \text{on } \mathcal{I} \quad (11b)$$

where Δh_c is the carbon–oxygen heat of combustion.

The last ingredient to complete the chemical model is the carbon balance equation. Since intragranular transport is not considered, the consumption of carbon is applied globally on a per grain basis. The shale grains are all supposed to initially contain the same volumetric amount of kerogen, and thus the same concentration C_g of carbon after pyrolysis has taken place. During the combustion process, this amount is decremented for each grain according to the reaction rate on its surface,

$$\frac{dC_g}{dt} = -\frac{1}{V_g} \int_{\partial V_g} \mathbf{n}_I \cdot \mathbf{J}_O \, ds \quad (12)$$

where V_g is the grain volume, ∂V_g is its surface and ds is a surface element. The step function H_C in equations (9) or (11a) tests whether C_g is positive for each shale grain.

3.6 Summary

Given the various approximations which have previously been listed, the problem formulation reduces to equations (1) and (2) for the gas flow, equation (3) for the gaseous species transport and equation (6) for the thermal problem. The whole chemical process is summarized by the boundary conditions (11) and by the carbon balance (12), which also describes the evolution of the bed. These equations are supplemented with initial conditions, where the bed geometry, the distribution of the inert and reactive grains, and the initial temperature field are specified, and by global boundary conditions, which mostly consist of the imposed entry gas flow rate.

A last question may deserve to be asked this point, namely, *would it be possible to simplify this formulation any further, without sacrificing too much physics or cancelling microscopic mechanisms that we think are determinant?*

The answer is probably no. Recall that our main purpose is to give a detailed account of the coupling between the transport and reaction mechanisms on the microscopic scale. These local couplings are embodied in the expressions for the local species and heat fluxes in (3b) and (6a,b), and they obviously call for knowledge of the local velocity field.

It is conceivable to conduct numerical simulations on a 'coarsened' model, where a conceptual pre-integration of some local effects has been performed. For instance, capillary models are intermediate between the fully local approach and the extreme simplification of a continuous description. They could be represented by a wire-like capillary network, with effective transport coefficients for the capillaries and effective exchange and reaction coefficients associated with the nodes. This preliminary integration is of the same nature as the 'black-box' model described in section 3.5 for the representation of a complex set of intragranular reaction and transfer processes. However, it was supported in the latter case by the very large contrast between the typical length scales of the microporosity and macroporosity, whereas the length of the capillaries would be of the same order of magnitude as the whole reaction zone thickness. Hence, the standard requirements for an homogenization procedure are not satisfied, and it is very unlikely that a small set of coefficients could realistically describe the transfers and reactions that take place in a single pore between a few grains in the bed, independently of what happens one or two grain diameters away, under strong, transient thermal and concentration gradients.

Therefore, we think that the detailed level of description adopted here is necessary, even if ultimately one of the results might be the identification of semi-local sub-systems and the quantification of corresponding effective coefficients which may be used in an upscaled and numerically less demanding model.

4. Numerical model

This section is devoted to the description of the numerical model, which basically solves the equations given in section 3, in the setting described in section 2.1. For the sake of clarity and concision, we skip most of the technical details and validation tests, which are given in full by Debenest [2].

The numerical code is a very complex assembly of program units that take care of the various mechanisms. Several of them had been developed in earlier works, in different contexts, and were adapted to the present needs. Most of the borrowed material comes from Coelho [22] for the construction of grain packings and the solution of the Stokes equations, and from Sallès *et al.* [23] and Békri *et al.* [24] who designed the first version of the random walk simulator.

4.1 Geometrical models

Since the contrast between the typical microscale (grain size) and the whole domain size is very large, we focus on the central part of the bed and we assume that for this purpose, the medium can be regarded as transversally unbounded.

The bed geometry is described by a 3D array of cubic voxels, with size a^3 , which are entirely filled with either gas or solid phase. However, since only finite arrays can be handled numerically, the solid phase distribution is supposed to be spatially periodic. A parallelepipedic unit cell is generated, and an infinite medium is obtained by the juxtaposition of replicas of this unit cell in the directions x , y and z .

Our ultimate objective is to conduct simulations in 3D samples that mimic as closely as possible the microstructure of real grain beds. In the present case, the grains in the reference experiment are fairly monodispersed in size and regularly shaped. We chose to represent them by spheres with a constant diameter $\Phi = 600 \mu\text{m}$.

Realistic samples of randomly deposited grain packings can be obtained by use of the numerical tools described by Coelho [22] and Coelho *et al.* [25], which can simulate the sequential ballistic deposition of grains with arbitrary convex shapes and size distribution. An example of a spherical grain bed is shown in figure 3(a). The grid size $a = \Phi/12$ is chosen in order to provide a fairly detailed image of the pore space, and the sample size is $(8\Phi)^3$ so that the unit cell contents are representative (about 600 grains). In cases where the shale grains are mixed with sand grains, the nature of the grains is randomly set. Note that although the solid space as a whole is periodic, the distribution of the shale and sand grains does not have to be periodic. In practice, we set it randomly in a long series of cells, which makes the sample aperiodic from the point of view of the smouldering process, whereas the velocity field remains periodic and can be computed at reasonable cost on the unit cell.

The type of media shown in figure 3(a) was used for extensive calculations when realism was pursued. However, simulations have also been conducted in 2D configurations, such as the staggered array of cylinders shown in figure 3(b). This allowed easier tests of the numerical tools and a faster sweep of the parameters, but most importantly, an easier graphical display of the results.

4.2 Flow field calculation

The gas flow velocity field is determined by solving equations (1) and (2). The first version of the solver was designed by Lemaître *et al.* [26]. It makes use of an artificial compressibility method, with a finite difference scheme on a staggered marker-and-cell mesh. Its performances were greatly improved and a fourth order spatial discretization was introduced by Coelho [22].

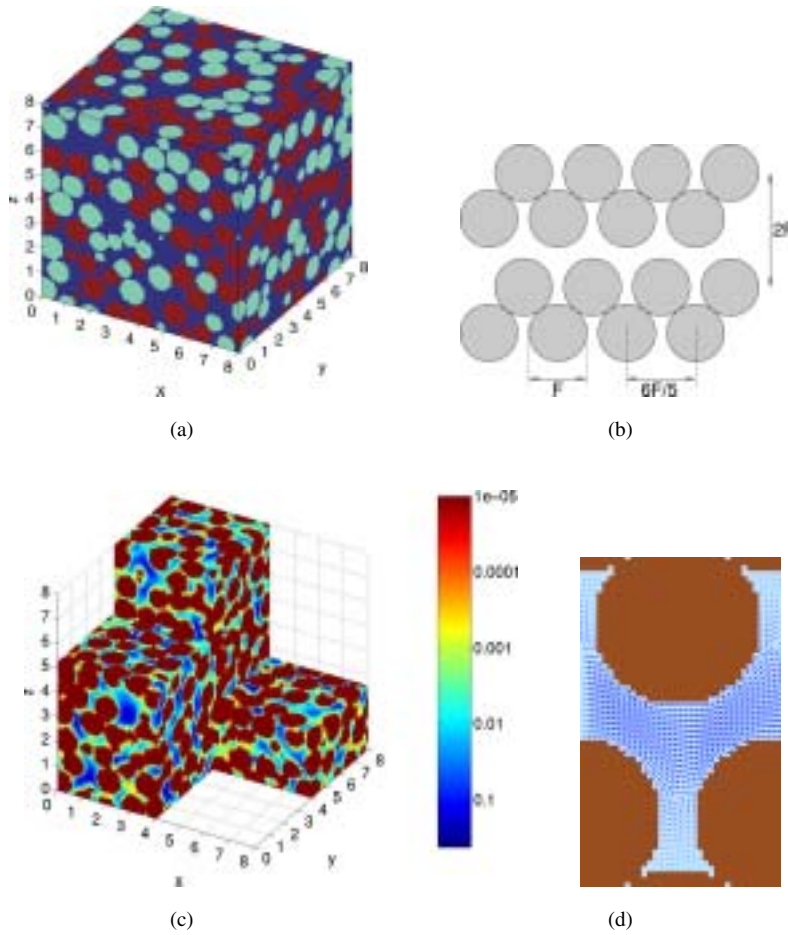


Figure 3. (a) Three-dimensional bed of randomly deposited spherical grains. The grain colours correspond to the type of solid material (shale or sand). (b) Two-dimensional geometrical model, composed of a staggered array of contacting solid cylinders. (c) Flow field in the sphere packing. The colour code corresponds to the magnitude of the velocity. (d) Velocity field in the array of cylinders. The dynamics of the velocity magnitude have been artificially reduced in order to reveal the flow structure with recirculations.

An excellent convergence of the velocity field (i.e. negligible residual velocity divergence) is required for a proper application of the random walk method described in the following section, which also requires a fourth order spatial discretization of the differential operators in equation (1). These technical points are discussed in detail by Debenest [2], who also examined the effects of inertia for moderate but non-vanishing Reynolds numbers ($Re \leq 10$), and confirmed that they do not strongly influence the flow structure.

Two illustrative examples of flow fields are presented in figure 3, in the 2D staggered array of cylinders and 3D sphere packing. The arrow plot for the 2D case shows the level of detail achieved in the flow description.

4.3 Random walk simulation of convection–diffusion in the gas

Both oxygen and heat transports by the flowing gas, which are described by the convection–diffusion equations (3) and (6a), are simulated by random walk algorithms. In this approach,

the transported quantity is represented by Brownian particles, whose trajectories are explicitly followed by elementary time steps, during which they undergo a deterministic displacement according to the local conveying fluid velocity and a random displacement which corresponds to the diffusion.

This technique has several advantages, which make up for its computational cost, when compared with a finite difference scheme. The main interest of Lagrangian random walk simulations is that they are free of numerical dispersion. This is a very important feature for the present problem, which involves complex 3D flows, and diffusive transfers both collinear and transverse to the local main flow direction. Another practical but decisive advantage in our case was that the core of the simulator already existed. We elaborated here on earlier implementations of such an algorithm in different contexts, about dispersion of a reactive solute in porous media or in fractures (Sallès *et al.* [23], [27]; Mourzenko *et al.* [28]; Bécri *et al.* [24, 29]). From these simulation tools, we kept the part that handles equation (13) with little changes. Substantial modifications and extensions were required for the present problem, but another practical benefit of the method is the relative ease with which new features, such as additional species or reaction mechanisms, can be added without need for a profound recasting.

As already stated, the extensive quantities (heat or chemical species) that are conveyed by the gas are represented by Brownian particles. Each of these stands for a quantum, for instance q_O moles of O_2 for the oxygen or q_T Joules for the heat. We also define the quantum q_C for the carbon, and we may introduce similar quanta for the various reaction products. The choice of the values of these quanta results from a compromise between the computational cost and the statistical stability, which both increase as the number of particles increases, i.e. when q_O or q_T decrease. In practice, q_C is set to the carbon content in a solid voxel. In addition, it is convenient to set the other quanta in accordance with the stoichiometry of the reaction (8).

The trajectories of the many particles of various nature are constructed by elementary time steps δt , during which they undergo a displacement $\delta \mathbf{r}$ which is the superposition of a deterministic convective component and of a random diffusive one

$$\mathbf{r}(t + \delta t) = \mathbf{r}(t) + \delta \mathbf{r} = \mathbf{r}(t) + \mathbf{v}(\mathbf{r})\delta t + \delta_d, \quad (13)$$

where \mathbf{v} is the conveying fluid velocity, and δ_d is a vector with a random orientation and a magnitude related to the diffusion coefficient D of the transported species (D_O for the oxygen, D_{Tg} for the heat) by

$$\delta_d = \sqrt{6D\delta t}. \quad (14)$$

The velocity \mathbf{v} is evaluated at the starting position $\mathbf{r}(t)$ of the particle by using a second-order Taylor expansion of the tabulated velocity field. For instance, for the x -component u ,

$$u(\mathbf{r}) = u_0 + \nabla u \cdot (\mathbf{r} - \mathbf{r}_0) + \frac{1}{2} (\mathbf{r} - \mathbf{r}_0) \cdot \nabla \nabla u \cdot (\mathbf{r} - \mathbf{r}_0), \quad (15)$$

where u_0 and the first and second gradients ∇u and $\nabla \nabla u$ are evaluated at the grid point \mathbf{r}_0 closest to \mathbf{r} . Note that this expansion requires a fourth order solution of the flow equation, for the consistency of the fluid and solute balance equations. In addition, a very good convergence of the solution for the velocity field is required, since any residual mass balance defect will result in errors in the transport simulation.

Cheaper computations are possible by using a formula of a lower order than equation (15), by keeping only its leading-order term or by linearly interpolating the velocity data between the grid points. However, either the velocity components or their first derivatives are then discontinuous across the cube's mid-planes or faces. This is a disturbing feature, which may induce depletions or over-concentrations of particles in these areas. Such expedients should

not be applied without care. The linear interpolation could be used in the staggered array of cylinders, due to the fine discretization $\Phi/a = 30$ and to the absence of any severe constriction of the flow path. All our 3D simulations have been conducted by using the most elaborate model (equation (15)).

The time step δt in equation (13) has to be set small enough in order to get accurate results. Both the convective and diffusive displacements should be kept smaller than the spatial resolution. For practical reasons, the same value of the time step is used to simulate the transports of all the chemical species and of heat. It is set so that the upper bound δ_M of the elementary displacements for oxygen never exceeds a threshold value smaller than half the grid unit a ,

$$\delta_M = \delta_{M,c} + \delta_d = \max(\|\mathbf{v}\|) \delta t + \sqrt{6D_O \delta t} = \frac{2a}{5}. \quad (16)$$

The convective and diffusive contributions to equation (16) depend of course on the Péclet number, but in all our simulations, typical values of δd are about $0.25a$ and $\delta_{M,c}$ is about $0.15a$. However, the convective displacement is in most cases much smaller than $\delta_{M,c}$, since $\max(\|\mathbf{v}\|)$ is generally 10 to 100 times larger than the mean velocity v^* .

The case when the particle displacement in equation (13) brings them onto the interface between the gas and solid domains has to be modelled with care, since it controls the thermal exchanges and the chemical reaction rates. Let us first describe the simpler case of the oxygen. Whenever a particle is displaced, we check whether it hits a solid surface during its flight. In that case, we test whether a chemical reaction occurs, whereby the particle would disappear, as described in section 4.5. If the particle survives, it immediately rebounds to complete its time step; the magnitude of the jump is proportional to the remaining fraction of δt to be performed.

The case of heat transport is different because heat can penetrate the solid. However, it turns out that the sequence described above for oxygen is also used for the thermal particles. For reasons that are described in section 4.4, any time a thermal particle hits a solid wall, we have to decide whether it will remain in the gas or enter the solid. In the latter case the particle disappears, and in the former one it is handled just as the oxygen particles, by completing its time step by a fractional jump. Note that thermal particles are also created at the solid walls, either as a result of a chemical reaction (see section 4.5), or because they are transferred from the solid.

Let us finally introduce a post-treatment which we use for the presentation of the results. The concentrations and the temperature are evaluated on the scale of the voxels a^3 . If such a cube contains n_O oxygen particles and n_T thermal ones, then

$$c_O = \frac{n_O q_O}{a^3}, \quad T = \frac{n_T q_T}{C_g a^3}. \quad (17)$$

Due to the stochastic character of the random walk approach, the instantaneous values of the local concentrations n_O and n_T are very noisy. Since the time step δt is very small, it is natural to consider time averages over a moving interval, corresponding to a large number of time steps but to a short period, compared to the time scales of the physical mechanisms. Hence, we define the smoothed quantity \hat{X} as

$$\hat{X}(t) = \frac{1}{\tau} \int_{-\infty}^t X(s) e^{(s-t)/\tau} ds, \quad (18)$$

where X may stand for T or the concentration of any transported species, and τ is a time constant. Simply put, \hat{X} is a time average, biased toward the current value, with a

memory that vanishes over a few times τ . The setting of this time constant is discussed in section 4.6.3.

4.4 Heat conduction in the solid

Heat transport in the solid material is purely conductive (see equation (6b)). It could be simulated by using the same random walk technique as in the gas phase. However, the treatment of the interphase exchanges is tricky, because of the very large contrast between the gas and solid thermal properties, with $D_{T,g}/D_{T,s} \sim 10^3$ and $C_s/C_g \sim 10^4$. None of the algorithms described in the literature (see Labolle *et al.* [30]) and references therein can put up with such extreme conditions, but by elaborating upon these earlier works, we could devise a numerical scheme up to the task. Since we do not use it in the current version of the simulation tool, it is not described in detail here, but we need to provide a few indications about it, because they are needed for the forthcoming description of the technique which is actually implemented. We just need to mention that when a Brownian particle hits the interface between the gas and solid domain, the probability that it will resume its flight on either side of the interface is proportional to the corresponding value of the effusivity, i.e. the product $E = C\sqrt{D}$. This is strongly biased towards the solid; with usual values of the thermal properties, the probabilities of re-emission towards the gas and towards the solid are

$$\mathcal{P}_g = \frac{E_g}{E_s + E_g} = 10^{-3} \sim 10^{-2}, \quad \mathcal{P}_s = \frac{E_s}{E_s + E_g} \geq 0.99. \quad (19)$$

A random walk simulator based on equation (19) has been implemented, and it gives quite satisfactory results. However, the large heat capacity of the solid relative to that of the gas imposes us to use a prohibitive amount of thermal particles and we finally adopted another approach. This scheme was only used for validation purposes.

Eventually, heat conduction in the solid is simply modelled by a finite volume scheme, with second order spatial discretization. An explicit time discretization is applied, with a step Δt much larger than the step δt of the random walk in the gas, because of the contrast in thermal diffusivity. The coupling of the radically different simulation algorithms in the gas and in the solid is implemented as follows.

During Δt , transfer from the gas towards the solid may happen any time a thermal particle hits a solid wall, with the probability \mathcal{P}_s given by equation (19). At the end of the time step Δt , the heat transfers between neighbouring solid cubes are taken into account, as given by the finite difference formulation, and the only missing ingredient in the heat balance is the transfer towards the gas from the interfacial solid cubes. These are evaluated as the number of thermal particles that would be expected to cross from the solid into the gas, if a random walk algorithm was applied in the solid. From the solid temperature, we get the number of thermal particles in the cube, and by simple geometric arguments, we can estimate how much of them would hit the solid/gas interface. Finally, the number of particles actually transferred to the gas is obtained by using equation (19). This completes the heat balance for the solid cubes, and an explicit time step is taken to update the solid temperature.

The newly created particles are subsequently handled just like the other ones by the random walk simulator. The period Δt is set so that at most one thermal particle is injected in the gas by an elementary surface element.

The performances of this rather atypical mixed technique have been carefully checked by Debenest [2]. It was shown to yield accurate results in a variety of 1D, 2D and 3D test situations, in static, stationary dynamic or transient regimes.

4.5 Chemical reaction

With all the previously described apparatus in place for the heat and chemical species transport, accounting for the main chemical process basically reduces to the following: any time an oxygen particle hits the surface of a shale surface element, on a grain that still contains carbon, the reaction (8) is implemented if the local temperature exceeds the threshold value T_r in equation (10). Since the number of hits per unit time and unit area is obviously proportional to the oxygen concentration nearby, and owing to the large energy of activation E , this procedure automatically satisfies the kinetic law (9).

Expressed in terms of the elementary thermal and chemical ‘particles’ and of the associated quanta q_i , the reaction (8) corresponds to



It is convenient to set the values of the quanta according to the stoichiometry of the reaction (8), i.e. $q_C = q_O = q_{CO_2}$ in moles. However, q_T was set smaller than the corresponding heat of reaction, with $N_T = 5$, in order to improve the signal to noise ratio of the temperature. The practical implementation involves the following steps.

- If a particle q_O hits a solid wall, we check whether the solid grain still contains some fuel, and whether the local temperature exceeds T_r .
- If no reaction occurs, the oxygen particle simply resumes its random walk.
- If a reaction occurs, the particle q_O and a quantity q_C of fuel are removed from the system; the amount of carbon in the solid grain is decremented by this amount.
- A particle q_{CO_2} of carbon dioxide is emitted on the gas side. Its subsequent transport can be simulated by the same procedure that is used for the oxygen.
- N_T thermal particles are emitted from the position on the solid/gas interface where the reaction took place. They enter the gas or the solid material, according to equation (19), and they are then handled by the procedure described in section 4.4.

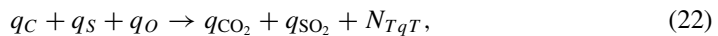
This scheme is sufficient to account for the chemical processes retained after the simplifying hypotheses formulated in section 3. However, it may be useful to provide here some hints about how extensions of the chemical model could be tackled.

The pyrolytic reactions which take place downstream of the oxidative reaction zone could be relatively easily incorporated, based on the following simple scheme



where q_K refers to a quantum of kerogen, and q_{CH_4} stands generically for gaseous pyrolytic products. This reaction would take place within the shale grains, with a probability per time step (resulting from the local temperature and from the kinetic law) for each kerogen quantum. The heat content of the solid elementary cube would be decremented by q'_T , and a quantum q_{CH_4} of gaseous product would be created.

Reactive components other than carbon in the shale, and their reaction products, could also be taken into account. This could be represented as



where q_S and q_{SO_2} stand generically for the other components and reaction products. Note that at our level of description, all the reactions are summarized in a statistical way in equation (22). A particle q_O represents a large number of oxygen molecules. When it reaches a solid interface, it reacts with both carbon and sulphur, which are intermixed.

A different approach could be used in other contexts. For instance, if we simulate waste incineration, we may face a larger number of components, with a coarser spatial distribution. Then, an oxygen particle can encounter solid bodies entirely constituted of different materials, and we may have to handle the reactions separately, with



where q_{Ci} and q_{Pi} represent one of the various components and its oxide.

4.6 Global management, boundary conditions, parameters of the simulations

Up to now, we have tried to give a full account of the ‘engine’ of the simulator, independent of its operating conditions. The present section is intended to fill in on case-specific aspects of the numerical simulations which have not yet been discussed.

4.6.1 Initial and boundary condition. The simulations are generally conducted starting from the ignition at $t = 0$, with the bed at room temperature. Then, stationary boundary conditions are maintained at the entry $x = 0$ and at the downstream boundary $x = L$ of a finite bed. Air at room temperature is injected at the bottom. On the downstream side, all the particles (heat, oxygen and other species) that reach $x = L$ are removed from the system. Adiabatic conditions are applied on the solid surface at $x = 0$ and $x = L$. Recall that periodicity conditions are applied in the directions transverse to the main gas flow. This means that the medium is regarded as transversely unbounded, or more realistically, that attention is focused on the bulk of the bed in a reactor whose diameter is much larger than the grain diameter Φ . Hence, transverse heat losses are not taken into account.

In a practical application, the smouldering process has to be somehow initiated, which necessarily involves pre-heating at the bottom of the column. We are not interested at this stage in this initial transient, which is design specific. Instead, we simply ignore the threshold temperature T_r in equation (10) for a while, and let the simulations run until a temperature profile sufficient to sustain the process has developed.

Obviously, the domain length L should be set large enough if any influence on the reaction zone is to be eliminated. Typically, the simulations are started with $L = 192\Phi$ in the 2D medium in figure 3(b) and with $L = 24\Phi$ in the 3D packing in figure 3(a). As the process goes, the influence of the downstream boundary starts being felt sooner or later in the reaction zone, and its position L has to be shifted farther away. This can become numerically very demanding, and an alternative technique, described by Debenest *et al.* [1], had to be designed. It is based on the matching of the 3D simulations up to L with a 1D macroscale continuous heat transport equation for $x > L$. The thermal sink can thereby be shifted as far downstream as necessary. Note that the downstream condition for the gaseous species transport poses no serious problem, because unlike heat, they do not accumulate in the solid and they are washed away by the gas flow.

4.6.2 Parameters. The simulations require many inputs, which can be roughly categorized into physical parameters, operating parameters, and a set of purely numerical ones without any physical relevancy.

The first group consists mainly of the physical coefficients of the constituents. Recall that as a rule they are taken at a temperature of the order of that prevailing in the reaction zone. We do not list their values here, because they are obviously case-specific. However, it is useful to

give the following typical orders of magnitude,

$$\frac{C_g}{C_s} \sim 10^{-4}, \quad \frac{D_{T,g}}{D_{T,s}} \sim 10^3, \quad \frac{E_g}{E_s} \sim 3 \times 10^{-3}, \quad \frac{U_F}{v^*} \sim 10^{-3} \text{ to } 10^{-4}. \quad (24)$$

The extreme values of the three first ratios have already been mentioned. They induce severe numerical constraints, and even dictated the choice of the simulation algorithm in some cases (see section 4.4). The last one is the ratio of the reaction front propagation velocity U_F to the mean gas velocity v^* , which partly determines the hierarchy of the time scales in section 4.6.3.

The volumetric amount and the properties of the kerogen in the oil shale is a very important parameter for the simulations, as well as for an actual experimental or industrial process. Three parameters are required in our simple chemical model, namely the threshold temperature T_r in equation (10), the volumetric amount c_C of carbon that remains after pyrolysis of the kerogen and the corresponding heat release when it is oxidized. The latter is set to $\Delta h_c = 395$ kJ/mol [21]. Measurements on oil shales from the same region as those considered in the experiment showed that the reaction (8) is initiated at about 500 K and that all the carbon is consumed at about 750 K [31]. Hence, T_r can be reasonably set in this range. Finally, in the absence of direct knowledge about c_C , a reasonable estimate can be deduced from the measured velocities U_F and \bar{v} and from the stoichiometric balance

$$\bar{v} c_O = (1 - \epsilon) p_S U_F c_C, \quad (25)$$

where p_S is the volume fraction of oil shale in the grain mixture. It is assumed here that both the carbon and oxygen are entirely exhausted in the process.

The operating parameters, i.e. the features that the operator of a physical reactor can act upon to optimize whatever criterion he wishes, mainly consist of the size (and in a lesser respect the shape) of the packed grains, the fraction p_S of oil shale grains in the mixture and the gas flow rate. We generally set $p_S = 1/2$ or 1 in the simulations, since ignition could never be performed in the physical model with smaller values. The gas flow rate is quantified by the Péclet number Pe_O (see equation (4)). We generally vary it from 2 to 10, which covers and exceeds the experimental range. Bubbling or partial fluidization of the bed occur if the flow rate is increased significantly further. Finally, the grain size Φ does not require a thorough exploration, because a similitude exists that allows the results obtained with a value of Φ to transpose to a bed with a different grain size, as can be shown by dimensional analysis (Debenest *et al.* [1]). Changing the inlet temperature by preheating the air is also an interesting avenue, but it was not investigated in this work.

The parameters in the final group are purely numerical. The most important ones, pertaining to the time scales, were thought to deserve a specific discussion, see section 4.6.3 below. Others are briefly mentioned here. Their lack of influence on the results, when properly set, was thoroughly investigated by Debenest [2].

The first is the grid step a for the spatial discretization, which should be small enough to account for the details of the microstructure, and for the small scale gradients of the temperature and pressure fields. The near identity of the results of 3D simulations with $\Phi/a = 8$ and 12 shows that these values are appropriate. On the opposite end of the size spectrum, the size of the periodic unit cell and the finite distance where the downstream boundary conditions are imposed should be large enough. The matching technique with a macroscale description on the downstream side solves the second problem. The real issue about the first one is the statistical representativeness of the unit cell contents. In the 3D calculations, it has dimensions $(8\Phi)^3$ and it contains about 600 grains. Coelho *et al.* [25] have shown that this is sufficient for a proper determination of the basic transport properties (conduction and flow) of deposited

grain beds. Finally, the only thing to consider about the discrete representation of the heat and chemical species by the quanta q_T , q_O and q_C is the balance between computational cost and statistical stability. As a rule, we set q_C so that the shale voxels initially contain one carbon particle, i.e. $q_C = a^3 c_C$. The other quanta are set according to the stoichiometry (see equation (20)). Recall that the smoothing in equation (18) greatly helps to improve the signal to noise ratio of the data.

4.6.3 Time scales. One specific problem is the coexistence of processes and events which take place on a wide range of time scales. Therefore, several time periods are introduced in the software. We detail here how they are set, in compliance with the physical mechanisms.

The time scales to be considered are related to the physical mechanisms which take place at various length scales. On the smallest one, a mean free time t_ξ of the order of 10^{-9} s is associated with molecular diffusion. All the time scales in our model, which is based on a continuous mechanics formulation, should be much larger than t_ξ . In particular, the ratio $\delta t/t_\xi$ has to be large if the random walk algorithm is to realistically simulate Fickian diffusion.

The next length scale is the discretization step a . A first set of time scales is associated with the diffusive and convective transports in the gas: $a^2/D_O \approx a^2/D_{T,g} (\sim 10^{-5}$ s) and a/v^* (10^{-5} – 10^{-4} s). The time step for the random walk has to be significantly smaller than these, in order to avoid spatial resolution losses

$$t_\xi \ll \delta t \ll \min(a^2/D_O, a^2/D_{T,g}, a/v^*). \quad (26)$$

In practice, δt is set so that the combined diffusive and convective jumps never exceed $2a/5$ (see equation (16)). Another time scale based on a is associated with heat conduction in the solid, $a^2/D_{T,s} (\sim 10^{-2}$ s). This is an upper bound for the time step Δt of the explicit finite differences scheme. However, there is a more stringent limitation. As discussed in section 4.4, we set this period so that at most one thermal particle is emitted to the gas per elementary surface element and per Δt . An approximate criterion for this is (with $N_T = 5$ and $\delta_M = 2a/5$)

$$\Delta t \leq \frac{10}{N_T} \frac{C_s}{C_g} \delta t \sim 10^4 \delta t. \quad (27)$$

This upper bound is always smaller than $a^2/D_{T,s}$. For the sake of numerical performance, there is no reason to set Δt much smaller than the bound in equation (27).

Consider now the physical microscale Φ , i.e. the grain diameter. The phenomena on this scale are mostly exchanges and redistributions. We have to consider the characteristic times τ_O for oxygen transfer from the bulk of the gas to the solid surface and τ_T for the thermal equalization of the solid and gas. Each of them is of the order of Φ^2/D , where D is an appropriate diffusion coefficient. They were determined by direct simulations by Debenest [2], and found to be of the order of 10^{-1} s. The smoothing constant τ in equation (18) has to be smaller than this in order to filter out only statistical fluctuations but to preserve real temporal variations of the concentration and temperature fields,

$$\tau \ll \min(\tau_O, \tau_T). \quad (28)$$

Finally, from a global point of view, the main time scale to be considered is the time $\Phi/U_F (\sim 1$ s) that it takes for the reaction front to progress by a distance Φ , and possibly for global features such as the peak temperatures or the width of the reaction zone to evolve. Results should be printed out with a period Δt_{out} smaller than that, but there is no point in analysing the data at intervals much smaller than the time a/U_F it takes the front to progress

by a , which is the spatial resolution of our description. In addition, τ should be smaller than Δt_{out} in order to avoid statistical overlap of the successive outputs. Hence, we set

$$2\tau = \Delta t_{out} = \frac{a}{U_F} < \frac{\Phi}{U_F} \quad (= 10^{-2}-10^{-1} \text{ s}). \quad (29)$$

In view of these criteria, the time periods in the simulations are generally set according to the following list:

- $\delta t \sim 0.1 \sim 1 \mu\text{s}$ step for the random walk algorithm in the gas,
- $\Delta t \sim 10^3-10^4 \delta t$ step for the finite difference solution of heat transport in the solid,
- $\tau \sim 10^5 \delta t$ time constant for the smoothing equation (18),
- $\Delta t_{out} \sim 10^5 \delta t$ period for the outputs of the simulation results.

Let us finally consider the delay between the instant when oxygen enters a grain and when it eventually reacts within this grain. Its typical value Δt_i can be evaluated as $\Phi^2/(4\bar{D}D_O)$, where \bar{D} is the effective diffusion coefficient of the porous grains. It can be roughly approximated by the square ϵ_i^2 of the intragranular porosity (Thovet *et al.* [32], Adler [33]), with $\epsilon_i \approx 0.15$ in the present case. In view of equation (24), and with moderate values of Pe_O , Δt_i is much smaller than the time scale Φ/U_F ,

$$\frac{U_F \Delta t_i}{\Phi} \approx \frac{1}{4\epsilon_i^2} \frac{U_F}{v^*} Pe_O = 10^{-3} \sim 10^{-1}. \quad (30)$$

Hence, the reaction front progresses during Δt_i by much less than a grain diameter, and therefore no significant change of the local thermochemical conditions can take place between the instant an oxygen particle enters a grain and the instant when it reaches its reaction site. This supports the simplification mentioned in section 3.5, whereby the oxidizer intragranular transfers are not explicitly described in the simulations.

5. Example of application and possible further extensions

Since this paper only describes a conceptual and numerical model but no extensive results, we do not attempt to provide any element of conclusion. Still, we wish to present at least an example of application, together with hints about the computational requirements and a brief survey of the extensions planned for the near future.

For illustration purposes only, figure 4 shows the temperature field in a 3D bed of grains, after a smouldering process has been simulated with $Pe_O = 10$ and $p_s = 1/2$ (left) or 1 (right), until the mean position of the reaction region has reached 26Φ or 17Φ , respectively. Without a detailed analysis, it is clear that the model captures the difference in the global behaviour which results from the difference in the bed composition. When $p_s = 1$, a hot temperature plateau develops downstream of the reaction front, whereas much more heat remains localized in the reaction zone when $p_s = 1/2$. The temperature then rises to higher values, and local thermal disequilibrium is more pronounced. These effects are fully analysed by Debenest *et al.* [1]. Note also the level of detail of the simulation, which provides complete thermochemical data on the microscopic scale.

Even though the domain size can be very large, of the order $3 \times 10^6 a^3$ in 3D calculations, storage is never the critical resource (about 300 MB in this case). Computational time is a more serious issue. It depends on the domain size, because of the simulation of heat conduction in the solid, and on the amount of fuel quanta, which determines the number of particles to handle in the random walk algorithms. In the conditions of figure 4 for $p_s = 1/2$, the front progresses by about 2Φ per day of computation on a 2.4GHz Pentium III Xeon processor (2D simulations

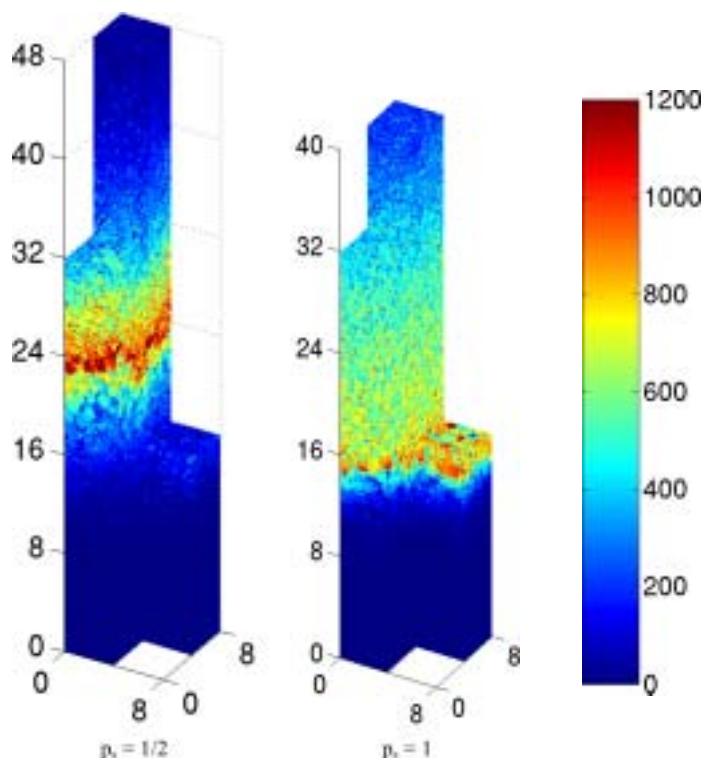


Figure 4. Temperature fields for smouldering simulations in a 3D grain packing, with $Pe_O = 10$ and $p_s = 1/2$ or 1, when the mean position X_F of the reaction zone is 26Φ and 17Φ , respectively. The gas flows in the ascending direction. The colour code for the temperatures in $^{\circ}\text{C}$ is given on the right.

are of course much faster). It should be noted however that computational optimization was not a priority during the development of the simulator, and significant speed-up is possible by different means. First, with the accumulated experience, the numerical parameters can be fine-tuned with great benefit. Micro-profiling of the numerical code should also be beneficial. Finally, part of the code could take advantage of a parallel execution.

The optimization of the performances is one of the most urgent tasks, but other improvements are also planned or already underway, which consist of complements to the model, especially from the chemical point of view. Most have already been mentioned. To begin with, pyrolytic reactions will be introduced. This is important since the recovery of their products is one of the motivations of many industrial processes. Avenues for various other enrichments of the chemical model have been mentioned in section 3.5. Of particular interest is the quantification of the emission rate of noxious species. All these extensions take advantage of the complete and detailed knowledge of the thermochemical conditions at the reaction sites. Finally, radiative transfers can probably not be ignored in some situations, and they will also be addressed in future works.

Acknowledgements

Most computations were performed at Centre Informatique National de l'Enseignement Supérieur (subsidized by the Ministère de la Recherche); whose support is gratefully acknowledged.

References

- [1] Debenest, G., Mourzenko, V.V., and Thovert, J.F., 2005, Smouldering in fixed beds of oil shale grains. Governing parameters and global regimes. *Combustion Theory and Modelling* (in press).
- [2] Debenest, G., 2003, *Simulation numérique tridimensionnelle, à la microéchelle, de la combustion en lit fixe de schistes bitumineux*, Ph.D. thesis, Poitiers.
- [3] Ahd, M., Bouhafid, A., Bruel, P., Deshaies, B., Maslouhi, A., Ouhroucheand, A., and Vantelon, J.P., 2000, Report on an experimental study of smoldering in packed beds of Moroccan oil shales, unpublished.
- [4] Ohlemiller, T.J., 1985, Modeling of smoldering combustion propagation. *Progress in Energy and Combustion Science*, **11**, 277–310.
- [5] Moallemi, M.K., Zhang, H., and Kumer, S., 1993, Numerical modeling of two-dimensional smoldering processes. *Combustion and Flame*, **95**, 170–182.
- [6] Lu, C., and Yortos, Y.C., 2000, The dynamics of combustion in porous media at the pore-network scale. Presented at ECMOR VII, Baveno, Italy, September.
- [7] Redl, C., 2002, In situ combustion modeling in porous media using lattice boltzmann methods. Presented at ECMOR VIII, Freiberg, Germany, September.
- [8] Hackert, C.L., Ellzey, J.L., and Ezekoye, O.A., 1999, Combustion and heat transfer in model two-dimensional porous burners. *Combustion and Flame*, **116**, 177–191.
- [9] Oliveria, A.A.M., and Kaviani, M., 2001, Nonequilibrium in the transport of heat and reactants in combustion in porous media. *Progress in Energy and Combustion Science*, **27**, 523–545.
- [10] Schult, D.A., Matkowsky, B.J., Volpert, V.A., and Fernandez-Pello, A.C., 1995, Propagation and extinction of forced opposed flow smolder waves. *Combustion and Flame*, **101**, 471–490.
- [11] Schult, D.A., Matkowsky, B.J., Volpert, V.A., and Fernandez-Pello, A.C., 1996, Forced forward smolder combustion. *Combustion and Flame*, **104**, 1–26.
- [12] Shkadinsky, K.G., Shkadinskaya, G.V., and Matkowsky, B.J., 1997, Filtration combustion in moving media: one and two reaction zone structures. *Combustion and Flame*, **110**, 441–461.
- [13] Aldushin, A.P., and Matkowsky, B.J., 1998, Rapid filtration combustion waves driven by combustion. *Combustion Science and Technology*, **140**, 259–293.
- [14] Aldushin, A.P., Rumanov, I.E., and Matkowsky, B.J., 1999, Maximal energy accumulation in a superadiabatic filtration combustion wave. *Combustion and Flame*, **118**, 76–90.
- [15] Aldushin, A.P., and Matkowsky, B.J., 2000, Diffusion driven combustion waves in porous media. *Combustion Science and Technology*, **156**, 221–250.
- [16] Whale, C.W., and Matkowsky, B.J., 2001, Rapid, upward buoyant filtration combustion waves driven by convection. *Combustion and Flame*, **124**, 14–34.
- [17] Akkutlu, I.Y., and Yortsos, Y.C., 2003, The dynamics of in-situ combustion fronts in porous media. *Combustion and Flame*, **134**, 229–247.
- [18] Deshaies, B., and Joulin, G., 1980, Asymptotic study of an excess-enthalpy flame. *Combustion Science and Technology*, **22**, 281–285.
- [19] Zhdanok, S., Kennedy, L.A., and Koester, G., 1995, Superadiabatic combustion of methane air mixtures under filtration in a packed bed. *Combustion and Flame*, **100**, 221–231.
- [20] Henneke, M.R., and Ellzey, J.L., 1998, Modeling of filtration combustion in packed beds. *Combustion and Flame*, **117**, 832–840.
- [21] Turns, S.R., 1996, *An Introduction to Combustion; Concepts and Applications* (New York: McGraw-Hill).
- [22] Coelho, D., 1996, *Génération, géométrie et propriétés de transport de milieux granulaires*. PhD thesis, Poitiers.
- [23] Sallès, J., Thovert, J.F., Delannay, R., Prevors, L., Auriault, J.L., and Adler, P.M., 1993a, Taylor dispersion in porous media. Determination of the dispersion tensor. *Physical Fluids A*, **5**, 2348–2376.
- [24] Békri, S., Thovert, J.F., and Adler, P.M., 1995, Dissolution of porous media. *Chemical Engineering Science*, **50**, 2765–2791.
- [25] Coelho, D., Thovert, J.F., and Adler, P.M., 1997, Geometrical and transport properties of random packings of spheres and aspherical particles. *Physical Review E*, **55**, 1959–1978.
- [26] Lemaître, R., and Adler, P.M., 1990, Fractal porous media. IV. Three-dimensional Stokes flow through random media and regular fractals. *Transport in Porous Media*, **5**, 325–340.
- [27] Sallès, J., Thovert, J.F., and Adler, P.M., 1993b, Deposition in porous media and clogging. *Chemical Engineering Science*, **48**, 2839–2858.
- [28] Mourzenko, V.V., Békri, S., Thovert, J.F., and Adler, P.M., 1996, Deposition in fractures. *Chemical Engineering Communications*, **148–150**, 431–464.
- [29] Békri, S., Thovert, J.F., and Adler, P.M., 1997, Dissolution and deposition in fractures. *Engineering Geology*, **48**, 283–308.
- [30] Labolle, E.M., Quastel, J., and Fogg, G.E., 1998, Diffusion theory for transport in porous media: transition probability densities of diffusion processes corresponding to advection–dispersion equations. *Water Resources Research*, **34**, 1685–1693.
- [31] Nabih, K., Boukhari, A., Real, M., and Arnada, M.A.G., 1998, Physical–chemical characterization of Tarfata's oil shale R sub-zones. *Annales de Chimie—Science des Mateiaux*, **23**, 389–393.
- [32] Thovert, J.F., Wary, F., and Adler, P.M., 1990, Thermal conductivity of random media and regular fractals. *Journal of Applied Physics*, **68**, 3872–3883.
- [33] Adler, P.M., 1992, *Porous Media. Geometry and Transports* (Stoneham: Butterworth-Heinemann).